Thermochimica Acta 591 (2014) 22–30

Contents lists available at ScienceDirect

Thermochimica Acta

journal homepage: www.elsevier.com/locate/tca

# Investigation on the status of rare earth elements contained in the powder of spent fluorescent lamps

G. Belardi [a], N. Ippolito [b], L. Piga [b,*], M. Serracino [a]

[a] Institute of Environmental Geology and Geoengineering (CNR) Area della Ricerca CNR, via Salaria km 29300, Monterotondo, Rome 00016, Italy
[b] Department of Chemical Engineering, Materials and Environment, Sapienza University of Rome, via Eudossiana 84, Rome 00184, Italy

ARTICLE INFO

*Article history:*
Received 7 May 2014
Received in revised form 15 July 2014
Accepted 16 July 2014
Available online 19 July 2014

*Keywords:*
Rare earth elements
Fluorescent powder
Hazardous material
Spent fluorescent lamps

ABSTRACT

The aim of this study is to examine the status of rare earth elements (REE) contained in the chemical compounds that make up the powder of spent fluorescent lamps, with a view of their recovery.
The status of REE in the as-received powder, as well as in a few size-class fractions of it, has been established. This way, only those size-class fractions containing high REE concentrations can be considered in a recovery process. The investigation has been carried out using particle-size, chemical, TGA/DTA, XRPD, SEM-EDS and EMPA analyses. The last technique enabled to establish the status of REE within the lattice of the chemical compounds present in the powder. The fineness of the as-received powder and the higher REE concentration in the finest size-classes suggest that physical methods of separation should not be used to separate the REE-containing chemical compounds from each other. Leaching methods seem more suitable with a material of such size.



## 1. Introduction

Spent fluorescent lamps contain both hazardous elements and valuable rare earth elements (REE) which at present are recovered to a very limited extent. The white powder which forms the inner coating of the glass tube of the lamp and emits visible radiations consists of REE-bearing particles. Due to their mercury content, fluorescent lamps are classified as hazardous wastes under the code 20 01 21 as per the hazardous waste list included in the European Waste Catalogue (EWC) [1]. The mercury content ranges from 1.5 to 5 mg/lamp depending on the lamp type and should always respect the limit established by the EU (5 mg/lamp). This limit is about 100 times less than the amount contained in the mercury thermometers recently banned from the market. Nevertheless, analyses of mercury content in different types of compact fluorescent lamps revealed mercury quantities per lamp up to 27 mg [2]. Table 1 reports the main applications [3,4] of REE together with the prices of their oxides [5]. The price trend of the REE treated in this paper, namely Y, La, Ce, Eu and Tb, is reported in Fig. 1 and depends significantly on the demand of various industrial sectors, on the mining production and supply restrictions practised by the major exporting countries. The main exporting country is China which owns 37% of the world's measured resources and, at present, it is also the largest exporter of REE worldwide [6], accounting for 95% of their mining production which includes few minerals such as bastnaesite, monazite and xenotime. As things stand, the recovery of REE from end-of-life devices from all consumer and business fields is of a strategic importance in supplying these elements. Evidence of this can be found in the main European research program "Horizon 2020" which has started this year and includes the recycling of REE and the development of new materials as substitutes or REE-compounds, among the topics of R&D in the area of raw materials.

As far as the recovery of REE is concerned, not much has been made so far. In fact, the fineness of the powder's particles makes the recovery of REE difficult and not achievable through simple and inexpensive processes, representing also a risk to human health [7,8]. It is known that physical methods of separation hardly apply to fine particles like those containing REE. In this case, hydrometallurgical methods could lead to better results although the complexity of this technique requires the use of expensive extraction reagents and the management of acidic solutions which have to be disposed off at the end of the process.

In any case, the characterization of the powder is preliminary to any physical or chemical valorisation process aimed at the recovery of the single REE or at the attainment of pre-concentrates which contain REE in higher concentrations than in the original material.

* Corresponding author. Tel.: +39 0644 585 629; fax: +39 0623 317 447.
*E-mail address:* luigi.piga@uniroma1.it (L. Piga).

http://dx.doi.org/10.1016/j.tca.2014.07.015
0040-6031/

**Table 1**
Main applications [3] and prices (2014) of rare earth elements and of their oxides [5].

| Element | Main applications | Metal ($/kg)[a] | Oxide ($/kg) |
|---|---|---|---|
| Cerium | Glass industry, ceramics, catalysts, metallurgy | 12 | 6[a] |
| Dysprosium | Automotive industry, ceramics, permanent magnets | 625 | 465[a] |
| Erbium | Glass colouring, amplifier in fibre optics, lasers for medical use | na | 72[a] |
| Europium | Phosphors, plasma screens, surgical use | 1225 | 925[a] |
| Gadolinium | Magnetic resonance, computer tomography | 132 | 46[a] |
| Holmium | Magnetic fields, laser for microwave equipment | na | 65[b] |
| Lanthanum | Fluid cracking catalysts, hydrogen storage batteries, laser crystals | 11 | 6[a] |
| Lutetium | X-ray phosphors | na | 1340[c] |
| Neodymium | Automotive industry, lasers, glass colouring, dielectrics, permanent magnets | 99 | 70[a] |
| Praseodymium | Ceramics, telecommunication systems, medical cat scans | 167 | 118[a] |
| Promethium | Beta radiation, light and portable X-ray sources, nuclear batteries | na | na |
| Samarium | Lasers, electronic equipment, microwave technologies, permanent magnets | 34 | 8[a] |
| Scandium | Ceramics, lasers, phosphors | na | 3350[b] |
| Terbium | Fluorescent lamps, X-ray phosphors, magneto–optic recording films | 980 | 790[d] |
| Thulium | Lasers, portable X-ray sources, microwave technologies | na | na |
| Yttertbium | Fibre optic technologies, lasers, thermal barrier systems | na | 50[e] |
| Yttrium | Ceramics, phosphors, plasma screens, automotive fuel consumption sensors | 62 | 21[f] |

na: not available.
[a] 99%/min, FOB, China.
[b] 99.5%/min, China.
[c] 99.9%/min, China.
[d] 99.9%/min, FOB, China.
[e] 99.99%/min, China.
[f] 99.999% min FOB, China.

According to a literature survey, not much work has been done on characterization of REE-bearing wastes. A brief characterization of the powder of fluorescent lamps is reported at the beginning of the papers which describe recovery processes of REE, however, they are far to be complete since characterization is not their main topic.

Chang et al. [9] studied REE with particle-size analysis, XRD analysis, UV analysis and reported some SEM images, but only halophosphate was found in the powder. Hirajima et al. [10] carried out particle-size analysis and zeta-potential measures aimed at assisting flotation tests. Yu et al. [11] carried out a characterization based on XRD and Raman spectroscopy, but on standards of high purity (>99.99%) only.

In this paper the characterization has been performed on a mix of powders of spent fluorescent lamps, coming from a discarded lamp processing facility. A complete investigation has been carried out on the status of REE present in the compounds which

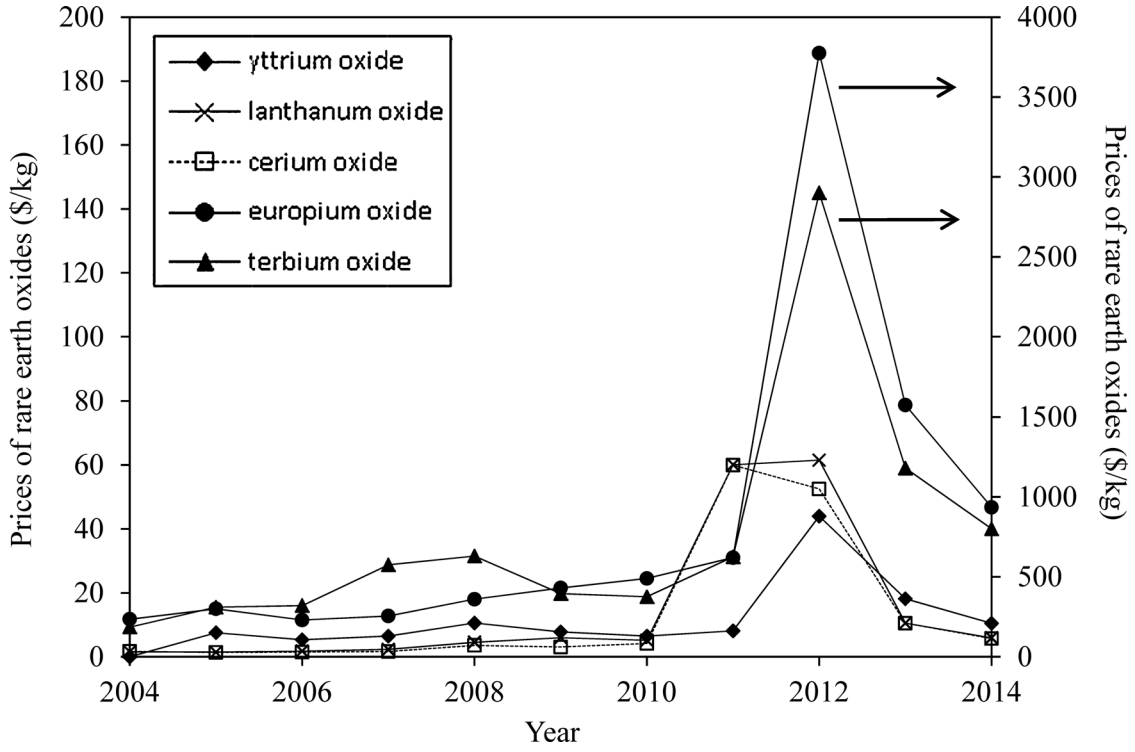


**Fig. 1.** Prices of the rare earth oxides investigated in the present paper.

constitute the powder, using various analytical techniques. Among these, the microprobe, never used before, enabled to determine the crystallo–chemical composition of the phases present in the powder. The results can lead to find the best methods for the recovery of REE. In fact, the knowledge of the compounds where the valuable REE concentrate allows the selection of those specific compounds which are to be treated in a recovery process.

## 2. Materials and methods

### 2.1. Material

A 10-kg sample of fluorescent powder was supplied by a recycling company that collects spent fluorescent lamps from authorized material recycling facilities or which are spread on the territory. The company recycles about 4 million lamps yearly and each tubular fluorescent lamp that is the commonest type on the market contains from 6 to 8 g fluorescent powder. Electrical contacts and the metal ends are removed from the lamps that are then crushed and the fluorescent powder separated from the glass. The powder is then heated in a retort at about 450 °C to remove mercury that is desorbed and recovered, and this makes the powder a non-hazardous waste to be disposed of in a less expensive landfill with lower environmental protection. The other components, like aluminium, copper, glass and the electronic parts are put on the market. About 47 t glass, 2.5 t aluminium and 6 t of non recyclables are obtained by the company for each t of powder whose production is about 20 t/y.

### 2.2. Particle-size analysis

About 500 g of the powder were screened into the following fractions: −2 + 0.150 mm, −0.150 + 0.075 mm, −0.075 + 0.053 mm, −0.053 + 0.038 mm, and <0.038 mm and each fraction was separately characterized. The finest fraction (<0.038 mm) was further analysed in wet mode with a laser particle-size analyser, model Sympatec Helos, equipped with He–Ne laser up to 0.9 μm and the results were elaborated together with those obtained by the sieves to reconstitute one class-distribution curve.

The same procedure was carried out after washing with distilled water of a sample of dried powder for 3 days and under stirring, in order to determine the percentage of water soluble components and to study the particle-size distribution after washing.

### 2.3. Chemical analysis

After sampling of the 10 kg, 3 samples of the powder after drying at 60 °C overnight were hand milled separately in an agate mortar to reach a fineness of 95% below 0.053 mm to ensure the complete subsequent fusion of resistate solid phases. 0.2 g of each sample was weighed in a graphite crucible with 1.3 g meta/tetraborate flux, fused in an induction furnace for 4.5 min and the melt was poured into 120 mL of 5% nitric and stirred continuously until complete dissolution (20 min). A robotic fusion system was used. The resulting liquids were analysed both by a Varian V735 ICP/OES and by a ICP/MS PerkinElmer Sciex Elan 6000. The same procedure was applied on the <0.038 mm fraction of each sample. The results of the chemical analysis of the two sets of samples permitted to reconstruct the chemical composition of the >0.038 mm fraction.

### 2.4. Thermal analysis (TGA/DTA)

DTA/TGA analyses were performed in a stream of air using a Stanton Redcroft Model 1500 thermobalance with a sensitivity of 1 μg, operating in the 20–1500 °C temperature range. The analyses were performed from 20 to 1000 °C at a 15 °C/min heating rate. Special care was devoted to maintain the same sample weight and geometry within the sample holder.

### 2.5. X-ray powder diffraction analysis (XRPD)

XRPD analysis was carried out on a diffractometer operating in reflection mode with $\theta$–$\theta$ geometry, equipped with high-resolution energy dispersive detector, opening at 3° in $2\theta$. Measurement parameters used were: $Cu_{K\alpha}$, 40 kV, 40 mA, scan angle ($2\theta$) = 0–70°; step width ($2\theta$) = 0.015°; counting time 0.3 s per step. Diffraction data were elaborated by EVA software.

### 2.6. Scanning electron microscope (SEM)

REE-containing powder was analysed with SEM using a FEI Quanta 400 MK2 model equipped with an energy dispersive X-ray spectrometer (EDS) Edax system, to determine the composition of the main phases that were clearly visible even at low magnification. Back-scattered electrons (BSE) were utilized to detect the contrast between areas with different chemical compositions, since heavy elements (high atomic number) backscatter electrons more strongly than light elements (low atomic number), which makes them brighter in the image. The operating conditions are reported in the SEM pictures shown through the text. A point-beam of 5–7 μm in size was used. The specimen was left in a metallizer at 1 Pa for 30 min and the surface was rendered conductive by sputtering a thin layer of graphite.

Digital images to determine the size-distribution of REE-bearing particles were acquired at not less than 2000× magnitude in BSE mode and were processed with Image-Pro Plus software.

### 2.7. Electron microprobe analysis (EMPA)

The mineral chemistry of the fluorescent powder was determined by using a CAMECA SX 50 electron microprobe, equipped with five WDS spectrometers and a EDS system Link eXL. The fluorescent powder was embedded, under vacuum conditions, in epoxy resin that was then lapped, pre-polished with abrasive powders and finally coated with a 200 Å carbon thickness.

All analyses were made using a 15 kV accelerating voltage and a beam current of 15 nA with a spot size of 1 μm. Measurements were carried out using a 30 s counting time for the main elements (30 s at peak position and 15 s at background) and 40 s counting time for minor elements (40 s at peak position and 20 s at background). Data were reduced with PAP Software [12].

Synthetic silicate glasses doped with RE oxides made at Manchester University were used as standards for REE. Standards for other elements used were: $YPO_4$ (Y,P), apatite (Ca, P), wollastonite (Si), corundum (Al), MgO (Mg), jadeite (Na), orthoclase (K), $BaSO_4$ (Ba, S), KCl (Cl), $TiO_2$ (Ti), $SrSO_4$ (Sr), InSb (Sb), vanadinite (V), fluorite (F).

The following crystals and radiations were used: TAP ($Na_{K\alpha}$, $Mg_{K\alpha}$, $Al_{K\alpha}$, $Si_{K\alpha}$, $Y_{L\alpha}$, $F_{K\alpha}$); PET ($V_{K\alpha}$, $P_{K\alpha}$, $S_{K\alpha}$, $Cl_{K\alpha}$, $K_{K\alpha}$, $Ca_{K\alpha}$, $Ti_{K\alpha}$, $Sr_{L\alpha}$, $Sb_{L\alpha}$, $Ba_{L\alpha}$, $La_{L\alpha}$, $Ce_{L\alpha}$, $Eu_{L\alpha}$, $Tb_{L\alpha}$); and LIF ($Mn_{K\alpha}$, $Fe_{K\alpha}$).

REE first order peaks are very close together and frequently overlap among themselves and with the secondary ones. Prior to quantitative analysis, each phase was identified with a full WDS scans to identify all the elements present in the samples to confirm the qualitative analysis carried out with SEM, to ensure that the peaks do not overlap, to determine the wavelengths for the measurement of the bottom of each peak and to choose the positions for background measurements.

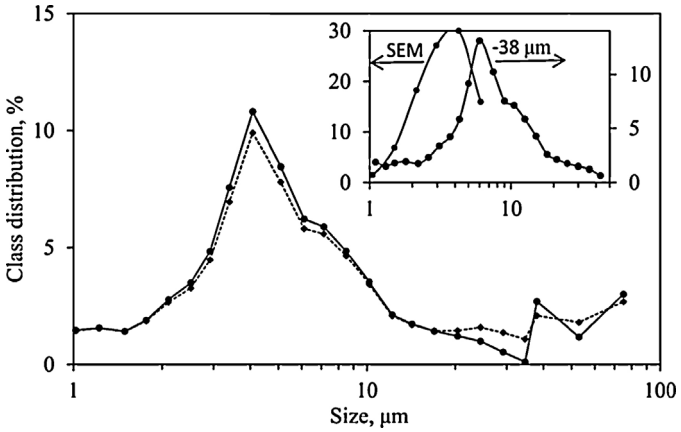


**Fig. 2.** Particle-size analysis distribution of the fluorescent powder as received (continuous line) and after washing (dotted line). The <38 μm particle-size analysis and the size-analysis of the REE-bearing particles as determined by SEM analysis, are also reported.

Analytical error were in the range of 1% for major elements and 5% for minor elements.

Many points were analysed on each phase present in the fluorescent powder but the average of the weight percentage of each oxide in each phase was calculated only considering the 5 analyses where the sum of the oxides was closest to 100%. The low values of the standard deviation of the average for all the analysed oxides assures the precision of the results obtained.

## 3. Results and discussion

### 3.1. Material

The preliminary screening, carried out on the powder, simulates the products obtained from valorisation treatments which yield concentrates that can differ considerably from tailing as regards to particle-size. Prior to analyses, the coarser fractions were ground to <0.053 mm to ensure homogeneity. 17.3 g of dried powder were immersed in distilled water under stirring and after drying and weighing of the residue, the soluble matters resulted to be 0.92 g (5.3%).

### 3.2. Particle-size analysis

Fig. 2 reports the results (continuous line) of the size-distribution analysis of the powder as received, after reconstitution of the coarse and the fine fractions that have been analysed with screens and with the laser-analyser, respectively. The analysis shows that 80% by weight of the material (the 80% of area under the curve) is characterized by a particle size less than 22 μm ($D_{80}$) and this results agree with that obtained by Hirajima et al. [10]. The coarsest three classes, namely 38, 53 and 75 μm, are characterized by a higher amount of powder respect to the adjacent smaller size-classes. This is due to the presence of glass in the powder that concentrates in the highest size-classes as also revealed by chemical and XRPD analyses.

The reconstituted size-distribution of the residue of the 17.3 g of washed sample (dotted line) is very similar to that of the unwashed sample.

Finally, in the frame within the same figure, the results of the size analysis carried out on the images of 596 REE-bearing particles acquired with SEM in BSE mode, is shown. This distribution shows that the size of all those particles is below 7 μm, therefore their recovery should be focused on the classes below that size that are about the 56% of the whole fluorescent powder as determined by the reconstituted size-distribution. The size-distribution of the <38 μm fraction of the powder carried out with the laser analyser is reported in the same frame as a comparison with the analysis carried out with SEM. This fraction is about 78% of the whole powder.

This fineness prevents the powder to be processed by physical methods to separate the particle containing REE among each other. Leaching methods are rather more suitable with materials of such a size.

### 3.3. Chemical analysis

#### 3.3.1. Chemical analysis of the sample as-received

Table 2 reports the complete chemical analysis of the powder as-received. As far as the major elements are concerned, CaO and $P_2O_5$ are present in higher concentration, 30.48 and 24.72% respectively, and this depends on the predominant presence of Ca and P-bearing phases. The presence of $SiO_2$, $Na_2O$ and $K_2O$ is due to the glass splinters coming from the fluorescent lamps and which are dragged in the powder during the dismantlement.

The low value of the loss on ignition, 1.14% at 950 °C, is due to the thermal treatment to which the powder was previously subjected in order to remove mercury. That loss includes $CO_2$ that is driven off during decomposition of calcite that is present in the sample as revealed by XRPD analysis.

Small amounts of Ba, Mn and Sb, are present within the lattice of the solid phases as determined by EMPA analysis.

A significant presence of REE as Y, La, Eu, Ce, Tb and to a lesser extent Gd, is evident. Yttrium was the predominant REE (49,260 mg/kg), while gadolinium was the REE with the lowest concentration (114 mg/kg) among the rare earth with concentration higher than 100 mg/kg and was not detected by other analyses but a few signals obtained by SEM investigation.

#### 3.3.2. Chemical analysis of the size fractions >0.038 mm and <0.038 mm

Figs. 3, 4 show the grade and the distribution, respectively, of the major oxides present in the powder, as a function of two particle-size fractions, >0.038 mm and <0.038 mm. The

**Table 2**
Chemical composition of fluorescent powder.

| Oxide | Dry solid (wt%) | Element | Dry solid (mg/kg) |
|---|---|---|---|
| CaO | 30.48 ± 0.36 | Sr | 2605 ± 24.1 |
| $P_2O_5$ | 24.72 ± 1.31 | Ba | 2233 ± 39.2 |
| $SiO_2$ | 21.28 ± 0.77 | V | 1538 ± 185 |
| $Na_2O$ | 3.87 ± 0.19 | W | 1021 ± 608 |
| $Al_2O_3$ | 3.34 ± 0.03 | Pb | 1009 ± 23.0 |
| MgO | 0.82 ± 0.03 | Zn | 276.7 ± 4.71 |
| $Fe_2O_3$ | 0.64 ± 0.13 | Cu | 216.7 ± 62.4 |
| MnO | 0.50 ± 0.01 | Zr | 153.7 ± 36.8 |
| $Sb_2O_3$ | 0.50 ± 0.008 | Ni | 106.7 ± 23.6 |
| $K_2O$ | 0.33 ± 0.008 | Cr | 36.7 ± 9.43 |
| $TiO_2$ | 0.04 | | |
| LOI* at 950 °C | 1.14 ± 0.10 | | |
| Total | 87.66 | | |
| Rare earth elements (mg/kg dry solid) | | | |
| Y | 49,260 ± 594 | Nd | 1.40 |
| La | 4583 ± 73.6 | Yb | 1.00 |
| Eu | 3957 ± 77.2 | Pm | 0.99 |
| Ce | 3383 ± 49.9 | Pr | 0.99 |
| Tb | 1320 ± 42.4 | Sm | 0.33 |
| Gd | 114 ± 1.70 | Dy | 0.30 |
| Lu | 8.8 ± 0.22 | Er | 0.20 |
| Sc | 3.0 ± 0.47 | Ho | 0.10 |

Three replicated samples were analyzed to determine the standard deviation that is reported after the average of each concentration; *loss on ignition.

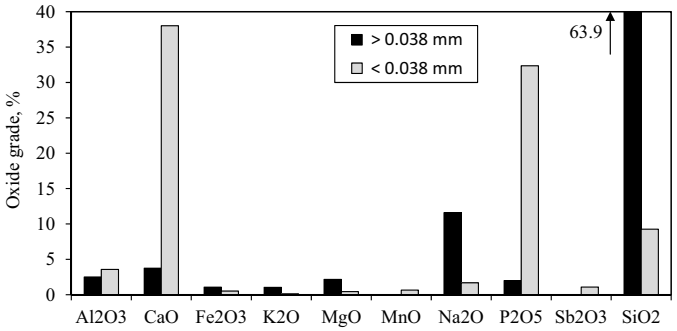


**Fig. 3.** Grade of the major oxides present in the <0.038 mm and >0.038 mm size-classes of the fluorescent powder.

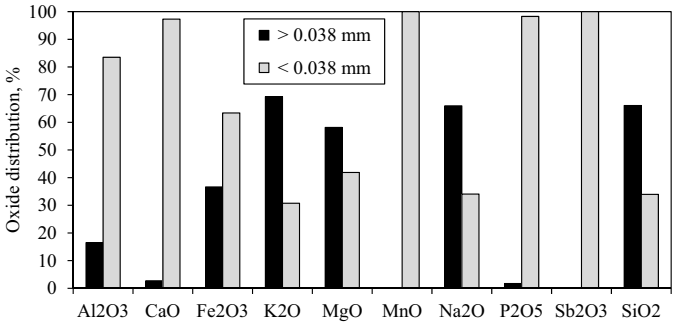


**Fig. 4.** Distribution of the major oxides present in the <0.038 mm and >0.038 mm size-classes of the fluorescent powder.

concentration of $SiO_2$ coming from the inner wall of the glass bulb is higher in the >0.038 mm fraction and the same behaviour show $Na_2O$ and $K_2O$ that are used as fluxes during glass production. On the contrary, higher concentrations of CaO and $P_2O_5$ are present in the <0.038 mm fraction owing to the fineness of the compounds that contain these oxides. The small amount of CaO found in the >0.038 mm fraction is probably to assign to carbonates as revealed by XRPD and TGA/DTA analyses. As far as the distribution between the two fractions is concerned, almost all of CaO, MnO and $Sb_2O_3$ concentrate in the <0.038 mm, while higher amounts of $SiO_2$, $Na_2O$ and $K_2O$ are present in the >0.038 mm fraction even though this fraction is about 3.5 times in weight less than the <0.038 mm fraction as revealed by the particle-size analysis.

Figs. 5, 6 show the grade and the distribution, respectively, of the REE and trace elements present in the same two particle-size

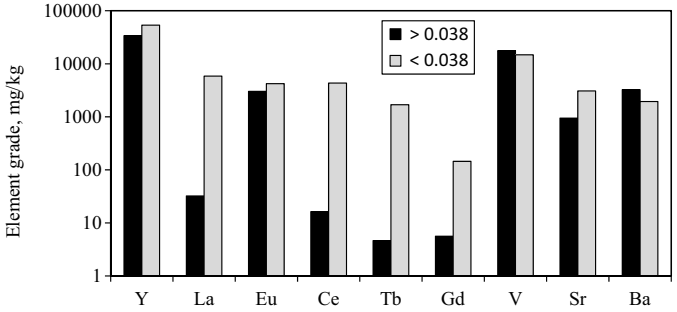


**Fig. 5.** Grade of the REE and of the trace elements present in the <0.038 mm and >0.038 mm size-classes of the fluorescent powder.

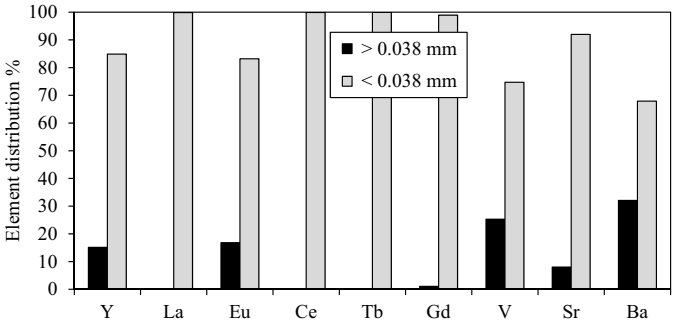


**Fig. 6.** Distribution of the REE and of the trace elements present in the <0.038 mm and >0.038 mm size-classes of the fluorescent powder.

fractions considered. Ce, La, Tb and to a lesser extent Gd show higher concentrations in the coarser fraction, while the concentrations of Eu and Y are of the same order of magnitude in the two fractions and the same behaviour have the trace elements, like Ba, Sr and V.

As far as the distribution of REE between the two fractions is concerned, Ce, La, Tb and Gd are almost completely contained in the <0.038 mm fraction while about 85% of Eu and Y are contained in the same fraction.

The results of chemical analysis of the fractions <0.038 and >0.038 mm show that the recovery of REE by leaching or physical methods of separation should be focused on the finest fraction so that most of the $SiO_2$, $Na_2O$ and $K_2O$ can be removed in advance. Nevertheless, the 15% of Eu and a bit more of Y would be lost in the coarsest fraction. In any case, the low size below which the REE concentrate confirms the difficulty of applying physical methods of separation for their recovery.

### 3.4. Thermal analysis results

The five particle-size fractions in which the sample of powder was divided, were analysed by TGA/DTA to investigate the behaviour of the powder fractions during heating. The TGA curves of the fractions, are reported in Fig. 7(a–e). All the particle-size fractions and to a lesser extent the fraction −2 + 0.150, that consists mainly of $SiO_2$, are characterized by a continuous loss of weight up to about 650 °C at which point the decomposition of carbonate starts for the fractions included between 0.150 and 0.038 mm and completes at about 730 °C. The presence of calcite is confirmed by the endothermic effect of the DTA, around 700 °C, of the fraction −0.053 + 0.038 mm reported at the bottom of the figure (f) as an example. The amount of calcite, determined by the loss of weight in the fractions −0.150 + 0.075 mm, −0.075 + 0.053 mm and −0.053 + 0.038 mm is 6.1%, 6.2% and 5.3%, respectively, and this indicates how calcite is homogeneously distributed among these middle size fractions while is hardly detectable and not detectable in the −2 + 0.150 mm and <0.038 mm fractions, respectively. A weighted average of the content of calcite as a function of the amount of all the size-fractions considered shows that the total content of calcite in the as-received powder sample is around 1.30% against 2.6% given by the LOI of Table 2 where other volatile compounds are probably included.

### 3.5. XRPD results

Fig. 8 shows the X-ray patterns of the fluorescent powder as-received and of a few size- fractions of it. At the bottom of the

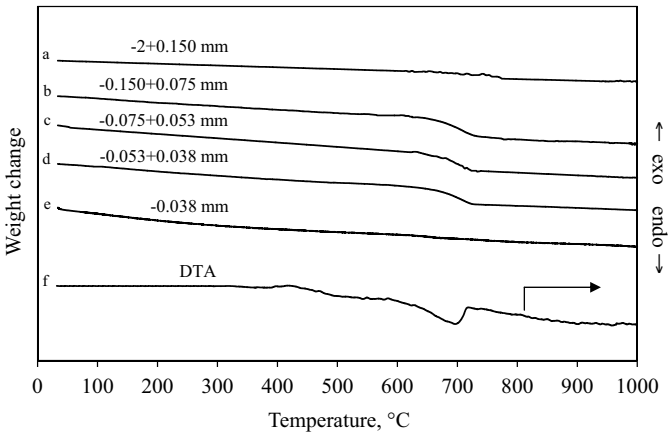


**Fig. 7.** Tg curves (a–e) of a few particle-size fractions of the fluorescent powder. DTA curve of the −0.053 + 0.038 mm fraction (f). Samples ground to less than 0.053 mm. Heating rate: 20 °C/min. Performed in a stream of air.

figure, the pattern of the powder as as-received is shown. Five species have been identified by the relative PDF files, namely fluorapatite or calcium-halophosphate ($Ca_5(PO_4)_3(F_{0.94},Cl_{0.1})$, PDF 01-084-1997), yttrium europium oxide ($(Y_{0.95}Eu_{0.05})_2O_3$, PDF 00-025-1011), wakefieldite ($YVO_{-4}$, PDF 00-017-0341), monazite ($CePO_4$, PDF 00-032-0199) and calcite ($CaCO_3$) that is hardly detectable. Nevertheless, calcite is clearly detectable in the >0.038 mm fractions as evidenced by the X-ray patterns of the four size fractions shown in the same figure. The amount of calcite and quartz decreases steadily as the particle size decreases up to <0.038 mm, at which point calcite and quartz are barely detectable. Quartz concentrates in the class between 0.053 and 0.038 mm and seems to be absent in the particle-size fractions greater than 0.075 mm even if $SiO_2$ is also present in those fractions as revealed by visual inspection and by chemical analysis. This apparent discrepancy could be due to the fact that in the upper classes $SiO_2$ is present as glass that being amorphous is not detectable by X-ray analysis. The presence of amorphous material is testified by the barely broad bump of the baseline between 10 and 40° of the coarsest fractions. The presence of quartz (crystalline $SiO_2$) could be due to an incomplete fusion of the silica sand, generally containing more than 98% quartz, used for production of the glass of the lamps.

The behaviour of wakefieldite is precisely the opposite of calcite and quartz, the amount present increasing in the finer fraction and decreasing in the coarser ones. Glassy components, apatite, Ce-phosphate and calcite were also found by Eduafo [13], while XRD analysis performed by Tunsu et al. [14] confirms the presence of yttrium and europium as yttrium europium oxide.

Monazite, yttrium oxide and fluorapatite that contain most of REE concentrate in the <0.038 fraction, and are absent in the upper classes. This technique confirms that the recovery of REE should be circumscribed to the treatment of the finest particles present in the powder.

### 3.6. Scanning electron microscope results

Fig. 9 shows a micrograph of a chip of glass, a particle of calcium halophosphate and a particle of lanthanum–cerium–terbium phosphate. The glass chip has a bigger size than the other particles as already stated by chemical and particle-size analysis. The qualitative analysis of the elements present in the point indicated by the arrow shows the expected presence of Na, K and Ca. F and Cl are contained in the calcium halophosphate while the other phosphate contains La, Ce and Tb and not Ce alone as determined

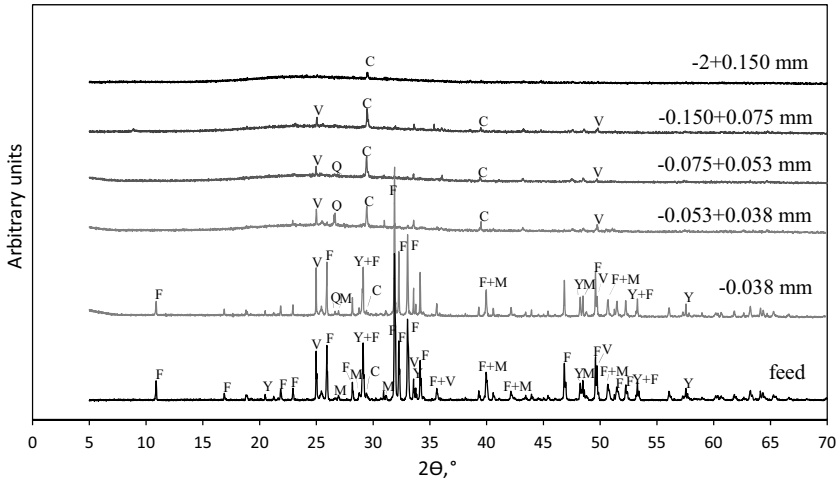


**Fig. 8.** X-ray diffraction patterns ($Cu_{k\alpha}$ radiation) of a few particle-size fractions of the fluorescent powder. F: fluoroapatite; Y: yttrium oxide; V: wakefieldite; C: calcite; M: monazite; Q: quartz.

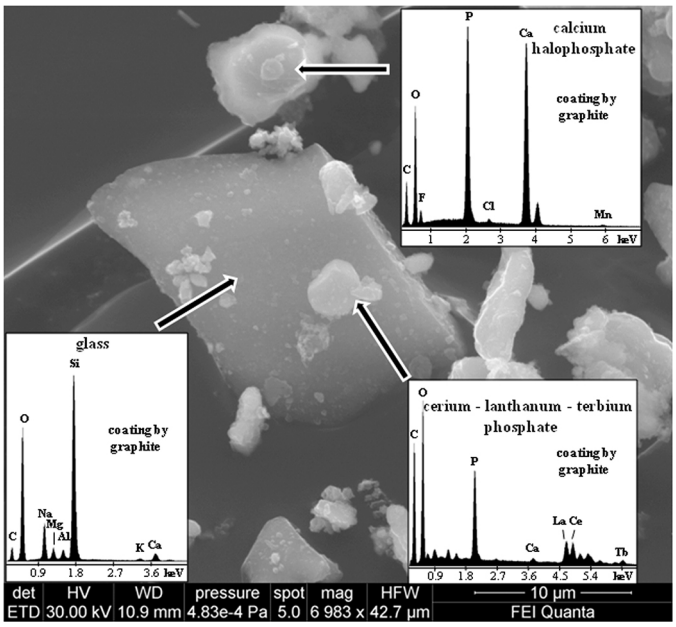


**Fig. 9.** Micrograph of the fluorescent powder. The qualitative analyses of glass, calcium halophosphate and cerium–lanthanum–terbium phosphate reported in the frames concern the points indicated by the arrows.

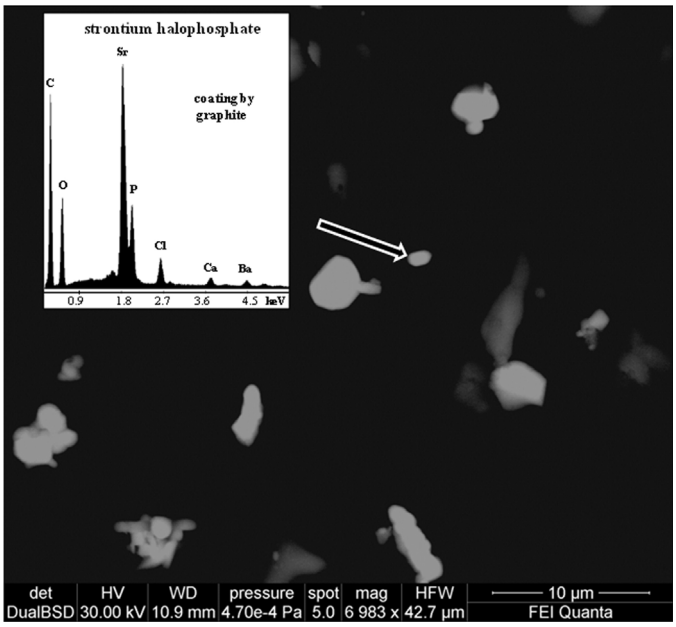


**Fig. 11.** Micrograph of the fluorescent powder. The qualitative analyses of strontium halophosphate reported in the frame concerns the point indicated by the arrow.

by X-ray diffraction analysis owing to the lack of the PDF file concerning the phosphate containing all the three elements.

Fig. 10 shows a micrograph of the oxides of yttrium and of yttrium–vanadium as it is easy to deduce from the qualitative analysis. Both oxides contain Eu as also revealed by the XRPD analysis in the case of yttrium oxide.

A micrograph and the qualitative analysis of strontium halophosphate is reported in Fig. 11. In Fig. 12 the micrograph of a rare and small particle of gadolinium oxide is shown with a particle of calcium phosphate that at this stage can be identified as a pyrophosphate ($Ca_2P_2O_7$) or as an orthophosphate ($Ca_3(PO_4)_2$) as reported by Hoekstra [15] that supports the presence of the pyrophosphate that seemed to give better properties to the fluorescent powder. Large globular particles of calcium halophosphate are also shown in the same figure. The peaks of C present in all the spectra are due to the thin layer of graphite used for rendering conductive the samples.

### 3.7. Electron microprobe results

On the basis of the qualitative analysis obtained both by SEM and by XRPD analyses, the proper settings of the microprobe could

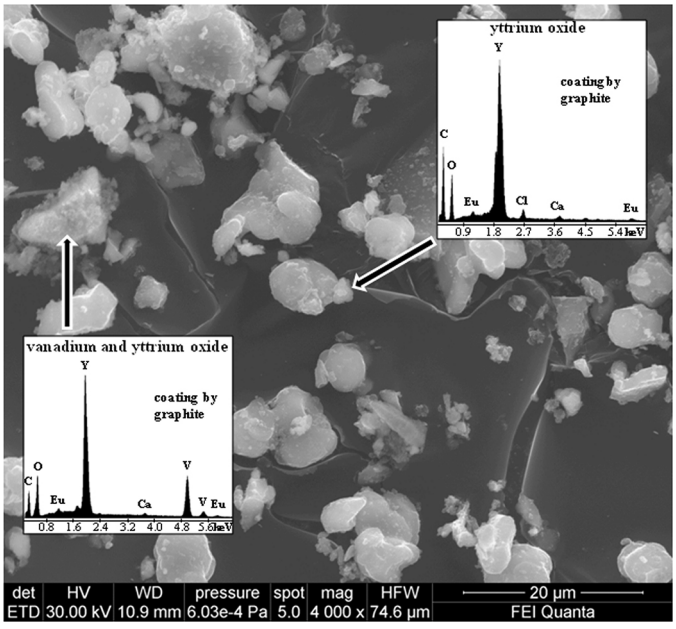


**Fig. 10.** Micrograph of the fluorescent powder. The qualitative analyses of yttrium oxide and vanadium–yttrium oxide reported in the frames concern the points indicated by the arrows.

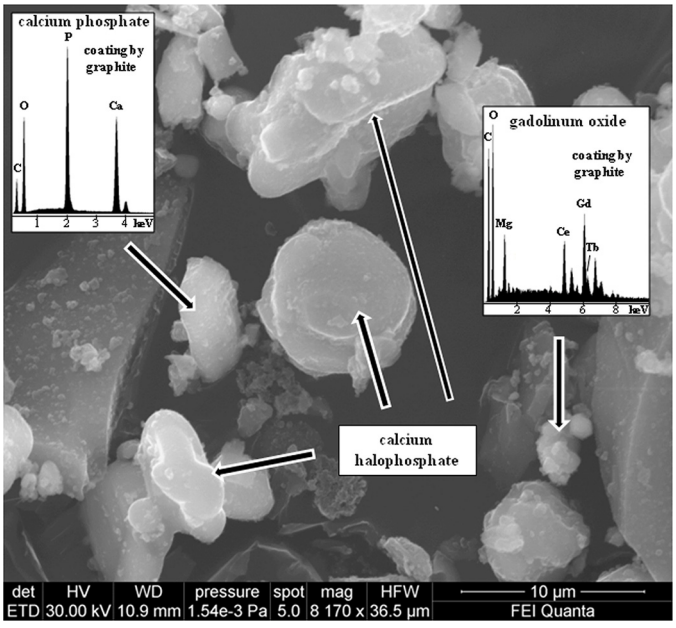


**Fig. 12.** Micrograph of the fluorescent powder. The qualitative analyses of gadolinium oxide and of calcium phosphate reported in the frame, concern the points indicated by the arrows.

**Table 3**
Chemical formulas of the main phases present in the fluorescent powder.

| | Oxide | Conc. (%) | σ (%) | Element | Conc. (%) | O conc. (%) | Chemical formula |
|---|---|---|---|---|---|---|---|
| Pyrophosphate | $P_2O_5$ | 55.25 | 0.99 | P | 24.13 | 31.13 | $Ca_2P_2O_7$ |
| | CaO | 44.76 | 0.49 | Ca | 31.97 | 12.79 | |
| Calcium halophosphate | $P_2O_5$ | 40.54 | 0.87 | P | 17.7 | 22.84 | $(Ca_{9.77}Mn_{0.17}Sb_{0.06})(PO_4)_6(F_{0.9}Cl_{0.1})_2$ |
| | $Sb_2O_3$ | 0.86 | 0.18 | Sb | 0.71 | 0.14 | |
| | CaO | 52.67 | 0.66 | Ca | 37.62 | 15.05 | |
| | MnO | 1.13 | 0.23 | Mn | 0.87 | 0.25 | |
| | F | 3.77 | 0.44 | F | 3.77 | | |
| | Cl | 0.68 | 0.13 | Cl | 0.68 | | |
| Lanthanum–cerium–terbium phosphate | $P_2O_5$ | 31.67 | 0.94 | P | 13.83 | 17.84 | $(La_{0.43}Ce_{0.44}Tb_{0.13})PO_4$ |
| | $La_2O_3$ | 28.55 | 0.65 | La | 24.34 | 4.21 | |
| | $Ce_2O_3$ | 29.89 | 0.46 | Ce | 25.53 | 4.37 | |
| | $Tb_2O_3$ | 9.53 | 0.72 | Tb | 8.28 | 1.25 | |
| Strontium halophosphate | $P_2O_5$ | 32.08 | 0.27 | P | 14.01 | 18.07 | $Sr_5(PO_4)_3(F_{0.9}Cl_{0.1})$ |
| | SrO | 65.64 | 0.37 | Sr | 55.50 | 10.14 | |
| | BaO | 0.67 | 0.03 | Ba | 0.60 | 0.07 | |
| | F | 0.75 | 0.33 | F | 0.75 | | |
| | Cl | 0.15 | 0.03 | Cl | 0.15 | | |
| Yttrium oxide | $Y_2O_3$ | 94.57 | 0.62 | Y | 74.46 | 20.10 | $(Y_{0.95}Eu_{0.05})_2O_3$ |
| | EuO | 5.58 | 0.54 | Eu | 5.05 | 0.53 | |
| Yttrium and vanadium oxide | $V_2O_5$ | 43.46 | 0.51 | V | 24.33 | 19.12 | $(V_{0.97}Eu_{0.03})(Y_{0.94}Eu_{0.06})O_4$ |
| | $Y_2O_3$ | 51.99 | 0.18 | Y | 40.91 | 11.04 | |
| | EuO | 4.06 | 0.09 | Eu | 3.80 | 0.40 | |

be selected that was equipped with an energy-dispersive detector, the proper crystals of the detector of the microprobe could be selected to quantitatively determine the stoichiometry of each phase present in the powder. The deviations from full-site occupancy of expected cations, as mainly revealed by X-ray analysis, and the presence of vicariant rare earth ions within the lattice of the phases was studied. In fact, the REE contained in the lattice of other phases cannot be recovered with physical methods of separation and the destruction of the lattice by leaching or thermal treatment is needed. Complete chemical analyses have been recalculated to mineral formula units that are shown in Table 3 and permitted to better study the REE-bearing phases. Yttrium oxide and wakefieldite (a mix of yttrium and vanadium oxides) bring all the Eu that substitutes both V and Y in the structure. Tb and Ba to a lesser extent, are contained in the cerium and lanthanum phosphate and the two elements are present in about the same molar amount. Halogen ions Cl and F are brought by the phosphates of calcium and strontium and the only phase with no vicariant ions is the calcium pyrophosphate that has been now precisely identified while the same analysis gave a generic calcium phosphate.

## 4. Conclusions

The investigation carried out on the powder coming from spent fluorescent lamps, which were collected by a recycling company, permitted to determine its size-distribution as well as its chemical and mineralogical compositions. The results show that about 80% of the powder has a size below 22 μm, while the rare earth element-bearing particles have a size below 7 μm. XRPD analysis permitted to reveal the main phases present in the fluorescent powder, namely calcite, fluoroapatite, monazite, quartz, wakefieldite, vanadium–yttrium oxide, and yttrium oxide. Most of $SiO_2$, $K_2O$ and $Na_2O$, coming from the glass of the lamp, distribute in the >38 μm size-fraction, while most of rare earth elements distribute in the <38 mm size-fraction.

The crystallo–chemical formulas of the rare earth element-bearing phases contained in the powder were established by an electron microprobe; Eu is contained as a vicariant ion in yttrium oxide and in vanadium–yttrium oxide, while Ce, La and Tb are present as phosphate. These pieces of information can guide the choice of the best process aimed at recovering the rare earth elements from the fluorescent powder. The fineness of the powder, in fact, would render very difficult the use of physical methods for the separation of rare earth element-bearing compounds or at least to obtain pre-concentrates of these compounds. Leaching methods to recover rare earth elements or their oxides would be more suitable with a material of such a size, after a preliminary screening of the powder at 38 μm to remove most of the $SiO_2$ (65%) and about 20% of the whole fluorescent powder.

## Acknowledgments

The authors want to thank both IRISAT srl (Italy) and Apliquim Brasil Recycle (Brasil) that made funds available for the implementation of the present work. A particular acknowledgement must go to Dr. Marco Albano for his support during SEM-EDS analysis.

## References

[1] Commission of the European Communities, Establishing a list of wastes pursuant to Article 1(a) of Council Directive 75/442/EEC on waste and Council Decision 94/904/EC establishing a list of hazardous waste pursuant to Article 1 (4) of Council Directive 91/689/EEC on hazardous waste, Off. J. Eur. Communities L 226 (2000) 3.
[2] E.J. Dos Santos, A.B. Hermann, F. Vieira, C.S. Sato, Q.B. Corrêa, T.A. Maranhão, L. Tormen, A.J. Curtius, Determination of Hg and Pb in compact fluorescent lamp by slurry sampling inductively coupled plasma optical emission spectrometry, Microchem. J. 96 (2010) 3–27.
[3] C.K. Gupta, N. Krishnamurthi, Extractive Metallurgy of Rare Earths, CRC Press LLC, London, 2005.
[4] K. Binnemans, P.T. Jones, B. Blanpain, T.V. Gerven, Y. Yang, A. Walton, M. Buchert, Recycling of rare earths: a critical review, J. Cleaner Prod. 51 (2013) 1–22.

[5] www.asianmetal.com/price/initPriceListEn.am?priceFlag=6, (accessed 27.02.14).
[6] X. Du, T.E. Graedel, Global use in-use stocks of the rare earth elements: a first estimate, Environ. Sci. Technol. 54 (2011) 4096–4101.
[7] A. Palasz, P. Czekaj, Toxicological cytophysiological aspects of lanthanides action, Acta Biochim. Pol. 47 (4) (2000) 1107–1114.
[8] W. He, G. Li, X. Ma, H. Wang, J. Huang, M. Xu, C. Huang, WEEE recovery strategies and the WEEE treatment status in China, J. Hazard. Mater. 136 (2006) 502–512.
[9] T.C. Chang, S.F. Wang, S.J. You, A. Cheng, Characterization of halophosphate phosphor powders recovered from the spent fluorescent lamps, J. Environ. Eng. Manage. 17 (6) (2007) 435–439.
[10] T. Hirajima, A. Bissobombolo, K. Sasaki, K. Nakayama, H. Hirai, M. Tsunekawa, Flotability of rare earth phosphors from waste fluorescent lamps, Int. J. Mineral Process. 77 (2005) 187–198.
[11] J. Yu, L. Cui, H. He, S. Yan, Y. Hu, H. Wu, Raman spectra of $RE_2O_3$ (RE = Eu, Gd, Dy, Ho, Er, Tm, Yb, Lu, Sc and Y): laser-excited luminescence and trace impurity analysis, J. Rare Earths 32 (1) (2014) 1–4.
[12] J.L. Pouchou, F. Pichoir, "PAP" A new model for quantitative analysis, Rech. Aerospatiale 5 (1984) 349–367.
[13] P.M. Eduafo, Experimental investigation of re cycling rare earth elements from waste fluorescent lamp phosphors, Thesis for the Degree of Master of Science (Metallurgical and Material Engineering), presented at Colorado School of Mines, Golden, Colorado, 2013.
[14] C. Tunsu, C. Ekberg, T. Retegan, Characterization and leaching of real fluorescent lamp waste for the recovery of rare earth metals and mercury, Hydrometallurgy 144, 145 (2014) 91–98.
[15] A.H. Hoekstra, The chemistry and luminescence of antimony-containing calcium chlorapatite, Thesis/dissertation, Centrex Publishing Co., Eindhoven, 1968.